ANGULAR MODELING OF THE COMPONENTS OF NET RADIATION IN AGRICULTURAL CROPS AND ITS IMPLICATIONS ON ENERGY BALANCE CLOSURE

Fernando Paz[1], Ma. Isabel Marín[1], Jaime Garatuza[2], Christopher Watts[3], Julio Cesar Rodríguez[4], Enrico A. Yepez[2], Antoine Libert[5], Martín Alejandro Bolaños González[6]

[1] GRENASER, Colegio de Postgraduados, Campus Montecillo, Estado de México.

[2] Departamento de Ciencias del Agua y Medio Ambiente, Instituto Tecnológico de Sonora, Ciudad Obregón, Sonora.

[3] Departamento de Física, Universidad de Sonora, Hermosillo, Sonora.

[4] Departamento de Agricultura y Ganadería, Universidad de Sonora, Hermosillo, Sonora

[5] Programa Mexicano del Carbono, Texcoco, Estado de México

[6] Posgrado en Hidrociencias, Colegio de Postgraduados, Campus Montecillo, Estado de México.

Corresponding author: Martín A. Bolaños González (martinb72@gmail.com; bolanos@colpos.mx)

Key Points:

- Albedo and radiative temperature were estimated using a one-parameter sun-sensor geometry model across five agricultural crops.
- The experimental adjustments were good (albedo: $R^2 = 0.9971$, RMSE = 0.432; radiative temperature: $R^2 = 0.9967$, RMSE = 0.008).
- The net radiation flux at nadir is overestimated, which implies a mismatch of the footprint between the components of the energy balance.

Abstract

Efficient water management in agricultural crops is necessary to increase productivity and adapt to climate change. Evapotranspiration (ET) data are key to determine water requirements of crops and set efficient irrigation schedules. Estimating ET at regional scale (for example, in irrigation districts) is a technically complex task that has been tackled by using data acquired by remote sensors on satellites that can be validated with scaled up field measurements when area sources are matched. Energy and matter flux measurements using the eddy covariance (EC) technique are challenging due to balance closure issues, claimed to be due to the different footprints of the energy-balance components. We describe net radiometer footprints in terms of the sun-sensor geometry to

characterize the bidirectional distribution functions of albedo and thermal emissions. In this context, we describe a one-parameter model of the components of net radiation that can be calibrated with a single data point. The model was validated in an experiment with five agricultural crops at Valle del Yaqui, in Sonora, Mexico, using different sun-sensor geometry configurations. The results from the experimental fits are satisfactory ($R^2 > 0.99$) and support the use of the model for albedo and radiative (surface) temperature in order to estimate net radiation. The analysis of the implications regarding a mismatch among footprints of the components of the energy balance showed that net radiometer fluxes are most of the time overestimated implying that the closure problem could be solved using similar footprint as aerodynamic components of the energy balance.

Plain language summary

Accurately estimating crop evapotranspiration is important because the agricultural sector is the largest consumer of fresh water worldwide (more than 70%). Applying only what the crop requires is the first step to efficient water use. There are many methods and tools to accomplish this task, many of which use the information acquired by remote sensing, as well as energy balance models to estimate evapotranspiration on a regional scale. Here we present a model that uses a single parameter to estimate albedo and radiative temperature, which are key factors in making evapotranspiration estimates operational (one data) on large agricultural areas through the use of remote sensing, especially satellite imagery. Model and measurements are used to analyze the energy balance closure showing that footprint matching could potentially explain differences.

Keywords: radiative temperature, albedo, energy balance, OPM, BRDF, BEDF

1. Introduction

Surface evapotranspiration (water evaporation from soil and transpiration from plants) is a key process in the exchange of energy and matter between the atmosphere and biosphere. Its contribution to radiative forcing (through water vapor generation and cloud formation) associated to climate change is as important as carbon dioxide emissions from land-use change (Bala et al., 1997; Stoy et al., 2019). The geographic distribution and availability of water is the main limiting factor of vegetation growth in about forty percent of the Earth's surface (Nemani et al., 2003). Water management in irrigated agriculture poses significant challenges for monitoring the water requirements of agricultural crops. Although water requirements in individual agricultural plots can be reliably estimated using relatively simple techniques (Allen et al., 1998), the task is not that simple at the regional scale (e.g., irrigation districts).

Remote sensing technologies coupled with energy balance models have been explored as a means for developing methods to estimate ET (Bastiaanssen et al.,

1998; Roerink et al., 2000; Allen et al., 2007). Several authors have reviewed the different ET estimation schemes using remote sensing (e.g., Couralt et al., 2005; Kalma et al., 2008; Gowda et al., 2008; Zeng et al., 2018). They have shown that the major sources of error in estimations include the use of radiative temperature (Tr) in the 8-14 m interval, instead of the aerodynamic temperature of sensible heat flux (To); the relationship between net radiation (Rn) and soil heat flux (G); and the difficulties for the temporal and spatial scaling of fluxes.

Direct measurements of energy and matter fluxes are commonly carried out using the flux covariance technique (eddy covariance) (Baldocchi et al., 1988; Verma, 1990). In this technique, energy and matter fluxes are measured through the covariance of wind speed and temperature (sensible heat, or H) or water vapor (latent heat, or E, where is the heat of vaporization of air). The area of influence or footprint of such measurements is dynamic and varies with sensor height, wind speed and direction, morpho-structural features of vegetation, and atmospheric stability (Lecrerc and Thurtell, 1990; Schmid, 2002; Vesala et al., 2008). On the other hand, Rn has a constant footprint that depends on the viewing angle and observation height of the sensor (Schmid, 1997); G has a fixed geometric configuration of sensors (heat plates) on the ground, so that it also has a constant footprint. The different measurement footprints of the components of energy balance may account for the commonly observed issue of lack of closure, which ranges between 10 and 30% (Wilson et al., 2002). Foken (2008) estimated typical error between 5 to 50% of the components of the energy balance equation. This situation, in addition to the spatially-defined footprint of remote sensing products, calls to scale the EC flux measurements to make them comparable with data acquired by remote sensors (Chen et al., 2009; Wohlfahrt and Tasser, 2015). Different approaches have been used for scaling (by aggregation/disaggregation) flux measurements (Chehbouni et al., 2000; Anderson et al., 2008) with acceptable results; but they are difficult to replicate in practice due to the complexity of the parameterization (i.e. knowledge of geometry of crops and parameters for the partition of fluxes), which is not available when using remote sensing techniques at large scales.

Under the perspective of energy balance closure using EC it is necessary to match footprints of different components in order to have a correct evaluation of the closure problem (Schmid, 1997). For this reason, a valuable contribution to solve this problem is to have a simple model of the net radiation footprint under oblique views without knowledge of the geometry of vegetation or the partition of fluxes associated to this geometry. Although there are several models of footprint modelling of components of net radiation (Jiang et al., 2001; Colaizzi et al., 2010; Zhao et al., 2010; Du et al., 2020) for angular (directional) estimations, all of them require specific data of the geometry of crops that it is not available in remote sensing approaches. In this perspective a hypothesis to be tested is that the net radiometer footprint can be modelled using a model with one parameter (plus angular data), thus requiring one data (actual measurement) to be parameterized. This paper discusses the issue of energy balance closure resulting from differences in the components footprints. We

propose a model to characterize Rn in terms of the basic components: albedo and surface temperature/emissivity under a sun-sensor geometry. We discuss the development of the footprints of these components, based on a simple model parameterized under sun-sensor geometry considerations. As the worst balance energy closures are observed in crops (Stoy et al., 2013), the model proposed was validated in a field experiment with five agricultural crops at Valle del Yaqui, in Sonora, Mexico. The implications of the developed model are discussed for the energy balance closure problem particularly on consequences of using a fixed footprint for net radiation.

2. Materials and methods

2.1 Energy balance and net radiation

The balance of energy fluxes (all components expressed in W m^{-2}) on a surface is given by:

$$Rn = \lambda ET + H + G \quad (1)$$

Under certain conditions, ET can be estimated directly from Rn using the Priestley and Taylor (1972) coefficient (Garatuza et al., 1998). The balance energy closure (C_{EB} 1, generally) is given by (Stoy et al., 2013):

$$C_{EB} = \frac{\lambda E + H}{Rn - G} \quad (2)$$

A value of 1.0 denotes a perfect closure. The closure of energy balances is part of the quality control of eddy covariance measurements (Aubinet et al., 2000) and it has reviewed in several publications (Wilson et al., 2002; Foken, 2008; Stoy et al., 2013; Mauder et al., 2020). From the analysis of the closure problem in EC measurements (Wilson et al., 2002), this can be related to over estimation of available energy (Rn – G) or under estimation of aerodynamic fluxes (ET + H). The energy balance closure can be related to several causes (Wilson et al., 2002; Mauder et al., 2020): (a) errors in sampling with different source of areas of sensors, (b) systematic errors of the instrumentation used, (c) energy sources (storage components) not considered, (d) losses of contributions due to low or high frequencies, and (e) advection of scalars; principally.

In flux measurements with eddy covariance methods there are different footprints of the energy balance components for a given wind direction, with Rn, H, and ET sensors in a fixed position, across a homogeneous agricultural plot. Using footprint measurements to make inter-comparisons (interoperability) of energy balance components is only valid for uniform, dense vegetation. Arguably, uniform dense vegetation is not the norm in natural ecosystems but it may be achieved in agricultural crops. Figure 1 shows the geometric configuration of plants in a ridge-and-furrow agricultural plot, with alternating zones of bare soil and total coverage by the crop. The difference in the geometric arrangement of plants and the geometry of observations (footprints) creates heterogeneity (the footprints observe/measure different portions of vegetation and soil) in an otherwise "homogeneous" plot; this leads to important differences in measurements recorded previous to a uniform and dense condition over the entire plot.

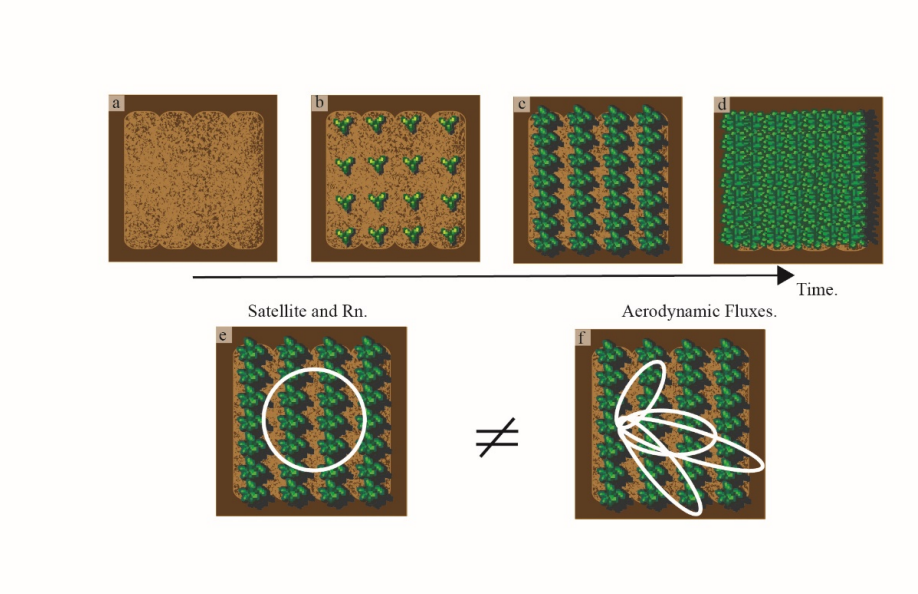

Figure 1. Geometric configuration of plants in a ridge-furrow agricultural crop across time (a, b, c and d) and the complex differences between footprint from different observations; e) satellite and *in situ* Rn measurements; f) flux-based methods such as eddy covariance.

The ground heat flux (G) component is measured using heat plates placed on the ground in a fixed geometric arrangement (see Figure 2) that results in a constant footprint. The sun-lit and shaded parts of soil and vegetation vary throughout the day and over the growth cycle in relation to crop growth and sun-sensor geometry. Thus, it is inadequate to assign equal weights to the different heat plate sensors when estimating G.

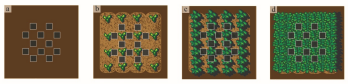

Figure 2. Arrangement of heat plate sensors on the ground for different growth stages (time progress) of a crop.

To estimate G, under a given geometric configuration of heat plate sensors, modelling plant growth in a crop field is relatively straightforward based on their shape, geometric arrangement in the plot, and sun-sensor geometry. Thus, the value of G corresponding to any footprint with a given orientation and

dimension is obtained as:

$$G_{\text{footprint}} = \frac{(\text{PMvi})(\text{Avi})+(\text{PMvs})(\text{Avs})+(\text{PMsi})(\text{Asi})+(PMss)(Ass)}{Avi+Avs+Asi+Ass} \quad (3)$$

where PM are average measurements over the sun-lit or shaded conditions, As are the areas of sun-lit or shaded conditions in the footprint, as indicated by subindices vi = sun-lit vegetation, vs = shaded vegetation, si = sun-lit soil and ss = shaded soil.

The components of net radiation are given by:

$$Rn = (Rs\downarrow - Rs\uparrow) + (Rt\downarrow - Rt\uparrow) \quad (4)$$

where Rs is short-wave solar radiation (W m^{-2}), Rt is long-wave (thermal) radiation (W m^{-2}). Arrows denote whether radiation is incoming (downwards) or outgoing (upwards).

Equation (4) can be reformulated using the Stefan-Boltzmann equation (Monteith and Unsworth, 1990), as follows (removing the arrows):

$$Rn = (1-\alpha)Rs + (\varepsilon_a \, \mathrm{T}_a^4 - \varepsilon_s \, \mathrm{T}_s^4) \quad (5)$$

where α is surface albedo (dimensionless), $_s$ is surface emissivity (dimensionless), is the Stefan-Boltzmann constant (= 5.67 x 10-8 W m^{-2} K^{-4}), $_a$ is air emissivity (dimensionless), Ts (K) is surface temperature, and Ta (K) is air temperature. Ts equals the surface radiative temperature.

Air emissivity can be estimated from (Brutsaert, 1982):

$$\varepsilon_a = 1.24 \left(\frac{e_a}{\mathrm{Ta}}\right)^{1/7} \quad (6)$$

where e_a is the vapor pressure of air (hPa).

Sun radiation data can be either obtained from weather stations or estimated using remote sensing (Garatuza et al., 2001).

Satellite-borne remote sensors measure the radiance (L) in thermal wave-length bands, from which temperature can be calculated using Planck's equation:

$$Lcn = \frac{C_1}{w^5 \pi \left[\exp\left(\frac{C_2}{\mathrm{wTb}}\right)-1\right]} \quad (7)$$

where Lcn (W m^{-2} m^{-1}) is black-body radiance (= 1), w is wavelength (m), Tb (K) is brightness temperature, C_1 = 3.74151 x 10^{-16} (W m^{-2}), and C_2 = 0.0143879 (m K).

Surface emissivity is calculated as the ratio between surface radiance (Ls) and black-body radiance (Lcn):

$$\varepsilon_s = \frac{\mathrm{Ls}}{\mathrm{Lcn}} \quad (8)$$

To simplify the description, in the discussion above we omitted the spectral ( ) and angular arguments. Accordingly, it is assumed that T, L, and are measured in a bandwidth similar to the longwave spectral region, or that this can be

estimated using small bandwidths. For albedo, the bandwidth corresponds to the shortwave segment of the electromagnetic spectrum (0.25-3 m).

Field measurements show that surface Tr varies with sun-sensor geometry: Ψ = (v, v, s, s), where denotes zenith angles and azimuth angles; v denotes viewing and s denotes sun illumination (Kimes, 1980; Mathias et al., 1987). Similarly, surface emissivity has angular effects similar to Tr (or Ls) (Salisbury and D'Aria, 1992; Cuenca and Sobrino, 1994). Considering both variables (Tr and), the bi-directional thermal emission distribution function (BEDF) (Jupp, 1998) should be known in order to model the angular effects of the sun-sensor geometry. Although different modelling schemes are available (Snyder and Wan, 1998; Smith and Ballard, 2001; Sobrino et al.; Du et al., 2020), all are difficult to parameterize, particularly with a single data point (one measurement). Angular variations in BEDF can be used to estimate sensible heat using two-source models (Chehbouni et al., 2001), but this approach it is not extended to net radiation components.

Field measurements show significant angular effects on surface albedo (Ranson et al., 1991). Therefore, it is necessary to model the bi-directional distribution function of reflectance (BRDF) or albedo. BRDF models (Wanner et al., 1995; Zhao et al., 2010) are also difficult to parameterize.

Finally, the relationship between the footprints of field measurements (Rn and G) associated to sun-sensor geometry should be determined. Figure 3 shows how the area (ellipses for oblique zenith angles and circles for a nadir view) of a sensor measurement changes according to the viewing zenith angle (the direction of the ellipse's major axis is a function of the viewing azimuth angle) for a given sun illumination condition. Paz and Marin (2019) show how to calculate geometry using the variables shown in Figure. 3.

Considering that aerodynamic footprints are larger than Rn and G (Marcolla and Cescatti, 2018), a mismatch problem (Schmid, 1997; Wilson et al., 2002), it is necessary to have similar footprints of all components of the energy balance. In crops and grasslands, Marcolla and Cescatti (2018) estimated that it is necessary to have a Rn sensor at height between 6-15 times higher than aerodynamic fluxes to have similar footprint areas, which bring new logistic and interpretation issues and yet do not consider angular variations in source areas.

The Rn footprint under nadir view is circular (Figure 1a); but for oblique views (changing view zenith angles) is elliptical (Schmid, 1997). Paz and Marin (2019) extended the circular footprint for this condition.

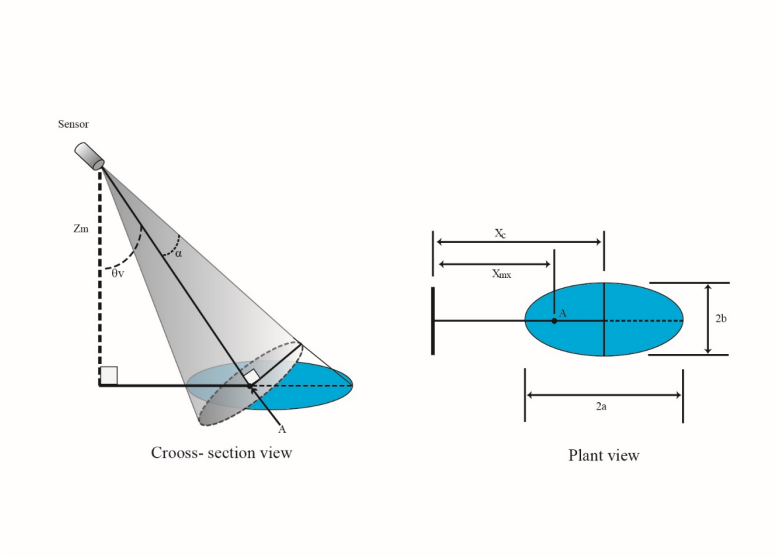

Figure 3. Footprint associated to the viewing geometry of the sensor where the footprint varies with view zenith angles (Paz and Marin, 2019).

2.2 One-parameter model for BRDF and BEDF

In this section we discuss how normalized spaces can be used to reduce complexity in measuring the energy balance of sun-sensory geometry components, as well as to estimate BRDF and BEDF, thus modifying the energy and matter balance equation.

The one-parameter model (OPM hereafter) for BRDF and BEDF is a modelling scheme that differs from other models currently used in operational applications of remote sensing. The OPM considers a particular symmetry (a hot spot, at the point where the viewing zenith and illumination angles coincide) which simplifies the modelling of BRDF and BEDF into a single parameter, so that only one data point (a single field measurement plus angular data) is required and applicable at the pixel level, for any satellite image acquired any time. The OPM was initially developed for modelling reflectance using particular symmetries for the different spectral bands (Bolaños et al., 2007); it was afterwards generalized into a single symmetry for all bands (Bolaños and Paz, 2010):

$$\begin{aligned} \chi &= 90 - \theta v + \theta s \\ Vn &= f(V)cos(\chi) \\ \chi &= a - gRn \end{aligned} \quad (9)$$

where V can be albedo, emissivity, or reflectance on any band in the shortwave electromagnetic spectrum, or radiative temperature on any thermal band; g is a parameter corresponding to BEDF or BRDF; and $a = 90°$. The function *f(V)* equals *ln (V)* when the scale effect is taken into account (that is, the area changes with the viewing zenith angle); *f(V)* equals V when the scale effect is

not considered.

Under the same assumptions, the BRDF or BEDF model defined by equation (9) can be extended to the case of azimuth angles:

$$\begin{array}{c} d\phi = \phi v - \phi s \\ If\ d\phi \leq 180,\ d\phi p = d\phi \\ If\ d\phi > 180,\ d\phi p = 360 - d\phi \end{array}$$

$$\begin{array}{c} If\ d\phi p \leq 90,\ \xi = d\phi p + \theta s \\ If\ d\phi p > 90, \xi = d\phi p - \theta s \end{array}$$

$$\begin{array}{c} gn = gcos(\xi) \\ \xi = A - G(gn) \end{array} \quad (10)$$

where G is the parameter corresponding to BRDF or BEDF and $A = 90°$.

The OPM allows parameterizing BRDF and BEDF with a single parameter: g for those cases where only the zenith angle (viewing nadir angle) varies, or G for the general case. Constants a and A equal 90° as a result of the symmetry implied by the position variables and .

The system of equations (9) and (10) can be reformulated ($a = 90,\ A = 90$) as:

$$f(V) = G\left(\frac{90-\chi}{90-\varsigma}\right)\left[\left(\frac{cos(\xi)}{cos(\chi)}\right)\right] \quad (11)$$

The OPM has been validated for reflectance measurements in experimental settings in laboratory (Cano et al., 2018; Paz et al., 2018), and with variations in the angular vision of satellite reflectance (Paz and Medrano, 2015 and 2016), while also being used to estimate more complex BRDF models (Medrano et al., 2013); with good results throughout (generally, $R^2 > 0.99$).

Statistics commonly used for the empirical assessment of the fit of the OPM to field data include the root mean square error ($RMSE$) and the mean absolute (relative) error (MAE):

$$\begin{array}{c} RMSE = \left\{\frac{1}{n}\sum_{i=1}^{n}\left(Tn, med - Tn, est\right)^2\right\}^{0.5} \\ MAE = \left\{\frac{1}{n}\sum_{i=1}^{n}\left|\frac{Tn, med - Tn,\ est}{Tn,\ med}\right|\right\} x100 \end{array} \quad (12)$$

Additionally, a simple linear regression was fit to the measured (med) and estimated (est, using the OPM) Rn values:

$$Rn, est = c + dRn,\ med \quad (13)$$

Parameters c and d, as well as the statistic R^2, were calculated for all the dates when albedo and radiative temperature were measured under different sun-sensor geometries.

2.3 Study area

The study was carried out in 2008 in an agricultural field located in Irrigation District 041-Río Yaqui, in Sonora, Mexico. The study area is located between coordinates 27°14'24"-27°16'48" N and 109°52'12"-109°54'36" W. The data obtained in the experiment were used for various studies, including the estimation of above-ground biomass and yield of crops (Pascual et al., 2012), modelling stress in crops (Reyes et al., 2011), biophysical and spectral scaling (Casiano et al., 2012), and modelling energy balances using satellite data (Chirouze et al., 2013).

Five homogeneous plots (PH) were chosen to characterize the footprint of and *Tr*. Plots were considered homogeneous since a single crop had been planted throughout the plot, on the same date, with a uniform planting density, and under the same furrow spacing and directions. The initial conditions of the selected plots are described in Table 1.

Table 1. Initial conditions of study plots

Plot	**Surface area (ha)**	**Crop**	**Furrow orientation**	**Furrow spacing (cm)**	**Plant height at the start of the experiment (cm)**
PH1		Bean	North-South		
PH3		Sorghum	East-West		
PH4		Chickpea	North-South		
PH5		Safflower	North-South		
PH6		Wheat	North-South		

2.4 Instrumentation

Two measurement schemes were used in each plot. The first scheme was aimed to characterize the footprint of α and *Tr* by simultaneously measuring crop reflectance and radiative temperature using different sun-sensor geometry configurations. The measurements were made using an *ad hoc* system consisting of the following:

1. A metallic stand for accurately positioning the height of each sensor. The stand consists of an extensible mast with clamping mechanisms at 2.5 m, 4.0 m and 5.5 m.
2. A polycarbonate structure with a flat base to support the Tr sensor. The structure was fitted with an electronic mechanism with servo motors to

accurately position the Tr sensor at any angle between 0° and 90° in the zenith plane (Figure 4a) and between 0° and 180° in the azimuth plane (Figure 4b).

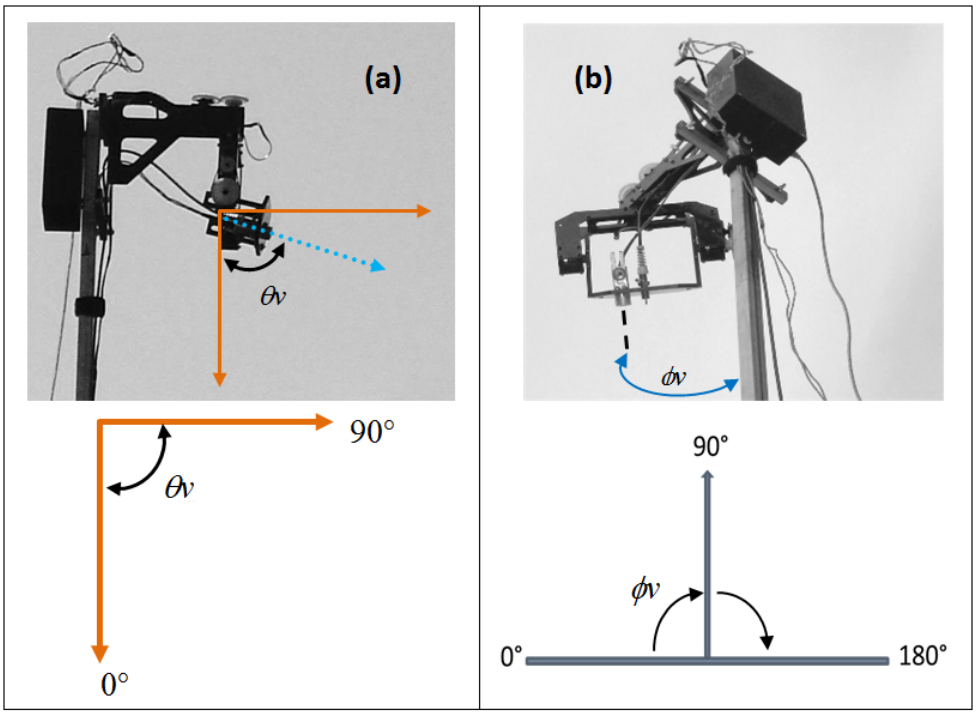

Figure 4. Geometry of the footprint-measuring device. (a) zenith plane, (b). azimuth plane

1. Control card and software for operating the polycarbonate structure.
2. Crop reflectance sensor. A hyperspectral (continuous data in 2 nm-wide bands on the 350 to 2,500 nm region) radiometer with 25° viewing angle (ASD^{TM}; FieldSpecFR Jr optical fiber),
3. Radiative temperature sensor for the crop. Apogee^{TM} model IRTS infrared thermometer with a 18.4° viewing angle (3:1 sensor height viewing: diameter ratio).
4. Console for System operation and data storage.

The measurement device was mounted on a tripod modified with a central support to stabilize the measuring system. A bubble level was used to maintain the tripod levelled; this ensured a vertical position during measurements (the equipment was disassembled at the end of each day and reassembled on the following day because of measurements rotation among crops). The measurement system was mounted with a 90° azimuth angle, parallel to the furrows direction. Ef-

forts were made for the measurement site to represent the conditions prevailing in the crop, avoiding any disturbance features. However, for practical reasons (transport, equipment assembly and disassembly), it had to be located towards one end (but several meters inside) of the plot, leaving a margin wide enough to prevent the measurements from being affected by adjacent bare soil surface A mark was left on each plot to easily locate the same site on subsequent weekly visits. The initial conditions of the study plots are described in Table 1.

2.5 Experimental design

Each experimental plot had a EC system but with only one heat plate or none for measurement G. Due to this lacking information no intent was done for energy balance closure estimation. A net radiometer (CNR1, Campbell Scientific) was placed at 3.0 m height connected to a datalogger (CR500, Campbell Scientific) for storage of measurement sampled at 10 Hz. All data were after averaged to half hour intervals.

The experimental campaign was carried out during the whole crop cycles, between February and May 2008. Each plot was visited once a week, and three measurement cycles of crop reflectance and radiative temperature were carried out on each visit. Measurements were made using the heights and viewing angles (v, v) listed in Table 2.

Table 2. Geometric parameters used for the measurement of radiative temperature and albedo.

Sensor height (m)	**Azimuth angle (v)**	**Zenith angle (v)**	**No. of readings**
2.5	15°, 45°, 90°, 135° y 165°	40°, 60°, 70°, 75°	20
4.0	15°, 45°, 90°, 135° y 165°	20°, 40°, 60°, 70°, 75°	25
5.0	15°, 45°, 90°, 135° y 165°	20°, 40°, 60°, 70°, 75°	25

As shown in Table 2, for a given sensor height and azimuth position, reflectance and radiative temperature readings were made varying the zenith position of the sensor. Thus, for example, with the sensor at 2.5 m height and 15° azimuth angle, four reflectance and Tr readings were made at zenith inclinations of 40°, 60°, 70°, and 75°. In total, 70 readings were made on each measurement cycle.

It should be pointed out that the azimuth plane of our system (Figure 4b) differs from the common practice (azimuth angles are positive in a clockwise direction from North). Azimuth used in the experimental measurements were using a value of zero perpendicular to rows of each crop field. The correspondence between the azimuth of the system and the actual azimuth depends on the location of the measurement site on each PH. All azimuths used on the field were changed to the standard notation and this convention is used in this paper.

The measurement cycles were carried out at different times of the day to obtain data for different solar angles (zenith and azimuth). The first cycle was

carried out in the morning, the second around solar noon and the third near sunset. Each measurement cycle was scheduled in advance so that they provide measurements: 1) representing three different sun zenith angles; and 2) with a difference of at least 10° between the selected zenith angles.

2.6 Measurement of footprints

Based on instrument positioning and geometrical angles, differences in expected source areas are illustrated in Figure 5 which depicts the footprints of reflectance and radiative temperature measurements, in relation to sensor height and viewing zenith angle. The parameters of ellipses that represent footprints are summarized in Table 3.

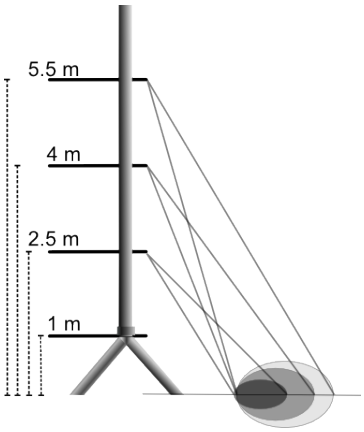

Figure 5. Footprints of reflectance and radiative temperature measurements for (a) a fixed height and varying viewing zenith angles, or (b) a fixed viewing zenith angle and different heights.

The parameters of ellipses representing the areas of influence of radiative temperature and reflectance are shown in Table 3, calculated according to Paz and Marin (2019). All measurements were made within homogeneous plots.

Table 3. Areas of influence of the Apogee^{TM} sensor for an 18.4º viewing angle and ASD^{TM} sensor for a 25° viewing angle with three different heights (parameters are described in figure 3).

Sensor	**Height (m)**	**v (°)**	**2a (m)**	**2b (m)**	**Area (m^2)**
Apogee					

ASD

2a = Major axis of the ellipse, 2b = minor axis of the ellipse

Vegetation albedo was estimated using the relationship between albedo and the spectral bands (B) of the ETM+ sensor on board Landsat 7 (Liang, 2000; Liang et al., 2002) (as proportions of reflectances):

$$\alpha = 0.356B1 + 0.130B3 + 0.373B4 + 0.085B5 + 0.072B7 - 0.0018 \quad (15)$$

From the spectral measurements for each band of the ETM+ sensor, reflectance values were estimated using the spectral response functions corresponding to this sensor. The response function provided by the manufacturer was used to estimate Tr.

A failure in the optical fiber of the ASD^{TM} sensor occurred several weeks after the measurements started. This failure interrupted the reflectance measurements for wavelengths below 1,000 nm. For this reason, we used the complete data set (n = 2,912) of the overall measurements to fit a multiple regression to estimate the relationship between albedo and bands B5 and B7 of the ETM+ sensor, as these were the only bands that could still be recorded after the optical fiber failure.

To estimate the albedo, a relationship was obtained using complete reflectance measurements and bands 5 and 7 of the ETM+ sensor ($R^2 = 0.954$) was (in %):

$$\alpha = 2.754 + 1.754B5 - 1.503B7 - 0.0140B5xB7 + 0.0202B7^2 \quad (16)$$

In order to analyze the albedo estimations under the optical fiber problem, Figure 6 compares the results obtained with the two models (15 and 16). The model fitted shows good agreement regarding the use of the complete model, with minimum bias.

[CHART]

Figure 6. Relationship between albedo values estimated using either all the spectral bands of the ETM+ sensor (complete model) or bands B5 and B7 only (truncated model).

3. Results

3.1 Model adjustments

To examine how Tr and α vary in relation to sun-sensor geometry, Figure 7 shows the measurements of above-ground coverage (fv) (Paz, 2018) made in PH4 (chickpea) between Julian days 59 and 129, with a coverage peak on day 80.

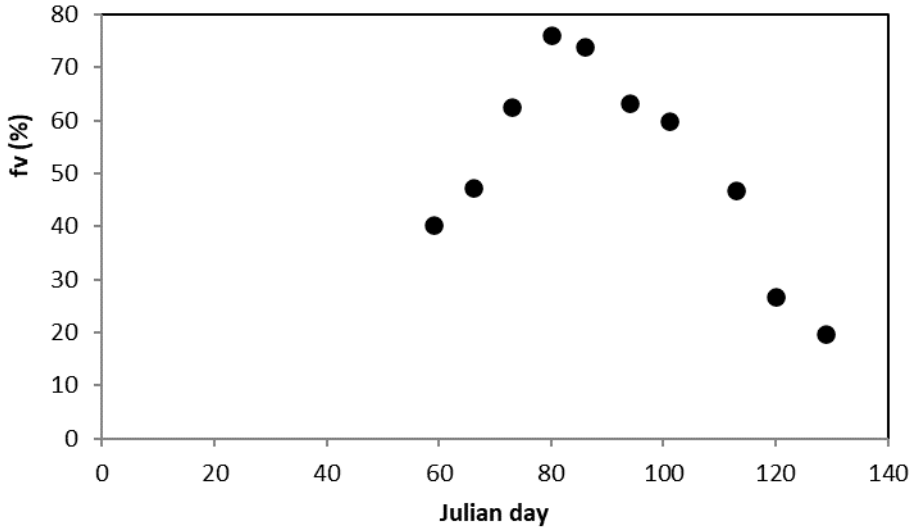

Figure 7. Temporal variations in above-ground coverage in PH4 (chickpea)

In order to analyze the use of the three different lighting conditions (morning, noon, and afternoon) used in the experiments, with various viewing azimuth and zenith angles (Table 2). Variations in Tr and α at the beginning and end of the measurements and during the fv peak are shown in Figure 8, for an observation height of 5.5 m.

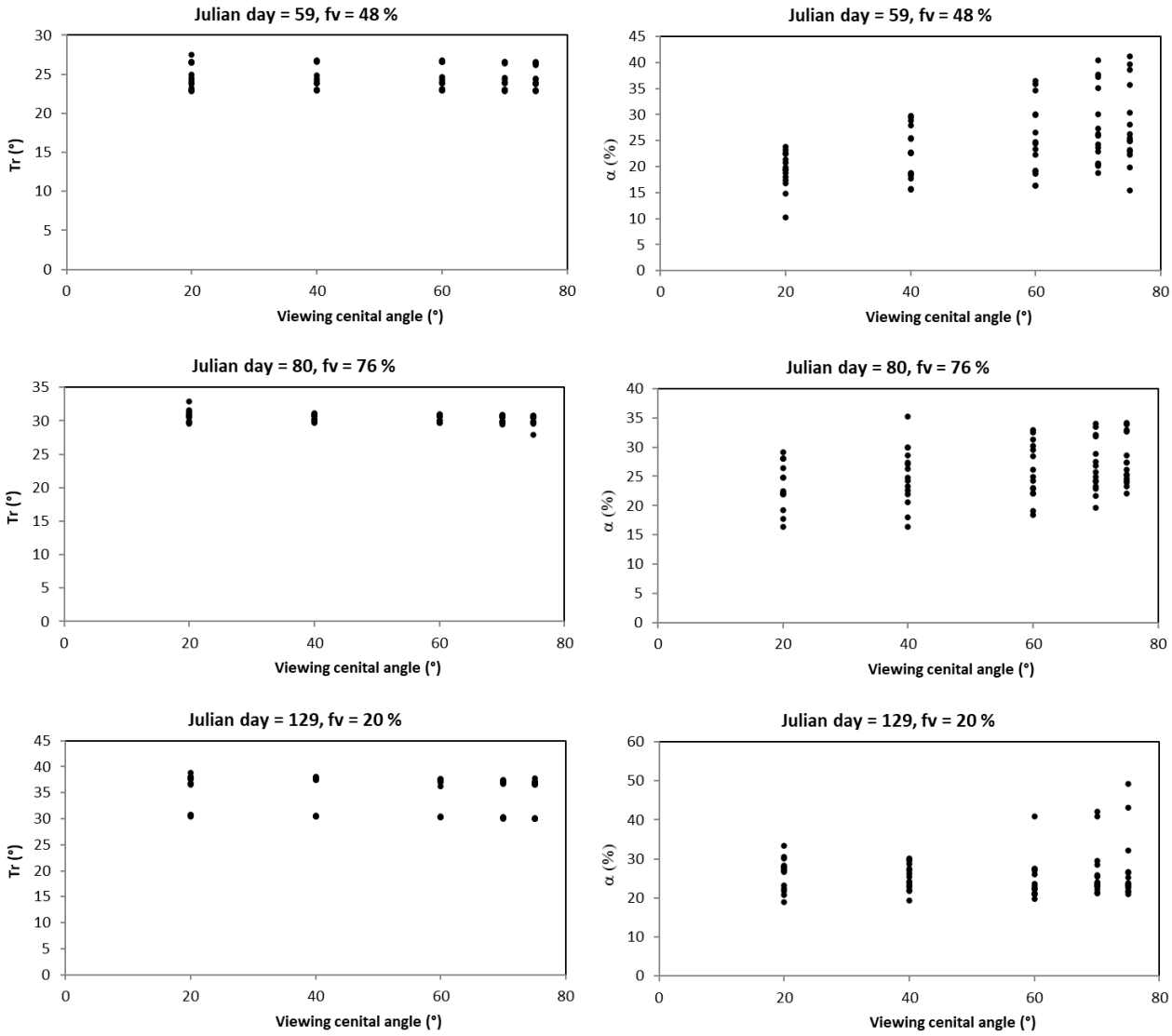

8. Variation of radiative temperature and albedo measurements in PH4 (chickpea), on three different days during the crop growth cycle.

The variations in radiative temperature were up to 10 °C and between 10 and 40% in the albedo values (Figure 8). This highlights the errors that can occur if measurements are not standardized to a common sun-sensor geometry (same footprint), which, in turn, may lead to large errors in energy flux estimates if the Rn (and G) footprint are different from aerodynamic fluxes.

The model of sun-sensor geometry was adjusted minimizing estimation error. Figure 9 shows the estimates of radiative temperature and albedo, normalized

(n) as per equation (12), for the case with no scale effect; Figure 10 shows the same for the case involving a scale effect.

[CHART]

[CHART]

Figure 9. Normalized estimates of radiative temperature and albedo for measurements in all PHs during the measurement campaign, with no scale effect.

[CHART]

[CHART]

Figure 10. Normalized estimates of radiative temperature and albedo for measurements in all PHs during the measurement campaign, including the scale effect.

3.2 Patterns of variation with view and sensor zenith angles

To explore albedo and radiative temperature measurement variations with footprint area (viewing zenith angle), under fixed solar illumination, Figure 11 show the patterns (solar zenith angle = 59.48°) for chickpea (PH4) in a day (only positive Rn measurements), depending in sun-sensor geometry (and crop grow), although the patterns shown in Figure 11 can change depending on fv. Nevertheless, the patterns shown are representative of conditions before maximum fv of the crop (minimum variations).

[CHART]

[CHART]

Figure 11. Variation of albedo and radiative measurements for chickpea (PH4) for Julian day 66.

Finally, two conditions (fv = 0 and maximum fv) were considered for the analysis of Rn patterns with solar illumination (solar zenith angle variation). The patterns are shown in Figure 12 for chickpea crop (PH4). The maximum value of Rn is around solar moon and it decrease in the morning and afternoon (solar zenith angles are higher than solar moon).

[CHART]

[CHART]

Figure 12. Variation of Rn measurements for chickpea (PH4) for Julian day 41 (bare soil) and 80 (maximum fv).

4. Discussion

4.1 Model adjustments

The results of the adjustment of the model to measured data show that including or excluding the scale effect has no marked impact on radiative temperature estimates. By contrast, in the case of albedo estimates, including a scale effect improves the experimental fit, as observed with other field measurements (Bolaños and Paz, 2010).

Overall, the OPM model for BRDF (albedo) and BEDF (radiative temperature) fitted adequately ($R^2 > 0.99$) the data from five agricultural crops, measured with different sun-sensor geometry configurations and at different growth stages. This supports the use of the model (one parameter) in operation with a single measurement, at field or satellite levels.

Using a sun-sensor geometry model (that implies a change to normalized space) can be used to estimate Rn footprint (see below), or to standardize Rn measurements to a fixed sun-sensor geometry, since knowing parameter g or G, equations (9) or (10), allows for estimates of any other sun-sensor geometry (angular arguments) analysis variables.

The OPM was developed for minimum data requirements using a transformed (normalized) space. Although the one-parameter model (OPM) can be used with agricultural crops, the problem of using only normalized estimates remains, as using the simple model to produce non-normalized estimates can lead to large errors resulting from the parameterization introduced (Bolaños et al., 2007). An alternative approach (no scale effect) consists in using the footprint model hereby proposed along with normalized values for all other components of the energy balance:

$$C_{\mathrm{EB}}\left[Rn \bullet cos(\chi) - G \bullet cos(\chi)\right] = \lambda E \bullet cos(\chi) + H \bullet cos(\chi) \quad (17)$$

This equation is exactly the same as equation (2). The scale effect implies a logarithmic function for transformations.

4.2 Patterns under sun-sensor geometry variations and their implications for the energy balance closure

Radiative temperature measurements decrease at higher zenith angles (as a smaller area of the soil is measured and the foliage contributions increase), whereas albedo measurements increase (as a larger area of vegetation foliage is measured and less soil is contributing). Additionally, the higher the vegetation cover (almost only foliage can be seen), the lower the variation associated with sun-sensor geometry. The OPM model, and experimental measurements of Rn (Figure 12), show that albedo variations with sun-sensor geometry are higher than radiative temperature measurements (Figure 11). Considering that conversion of Tr to Ts can be done using a simple adjustment (with atmospheric conditions and fv changing slowly) and the surface emissivity has an inverse pattern than Tr (Ts) when fv is less than maximum fv (the pattern change with high fv), but these variations are small (Jiang et al., 2001), if we use equation (5) then Rn decrease as footprint increase (view zenith angle increase) to match footprints of E and H. This implies that nadir measurements of Rn are ever

overestimated since C_{EB} is less than 1.0, as measured with EC systems (Wilson et al., 2002). In simple geometric terms, the elliptic footprint of E and H (normal case) requires a change from circular to elliptic footprint for Rn (this implies diminishing the value of Rn) so as to make correct energy and matter balances (Schmid, 1997).

If we used the reciprocity principle for BRDF or BEDF (Snyder 1998; Di Girolamo, 2003) interchanging solar zenith angles for view ones (Figure 12), then Rn is reduced when view zenith angles are increased (i.e. footprints are larger than nadir view angles as used in EC systems), leading to a mismatch between footprints and a lack of balance between components.

When evaluating the case of term (Rn – G) of the balance defined in equation (2), different authors, after considering different sources of errors associated to the closure of the energy balance, argue that spatial (and temporal) heterogeneity at landscape scale could be the cause of lack of energy and matter closure (Wilson et al., 2002; Foken, 2008; Stoy et al., 2013). In order to analyze variations of available energy (Rn – G) it is possible to simplify this term using the linear relation between Rn and G (Idso et al., 1975), although this can be more complex (Santanello and Friedl, 2003). For example, Su (2002) and Anderson et al. (2007) use the relation $G/Rn = c$, where c varies with fv. Using this relation, balance of energy of equation (17) can be modified:

$$C_{EB}\,[Rn \bullet cos(\chi) \bullet (1-c)] = \lambda E \bullet cos(\chi) + H \bullet cos(\chi) \quad (18)$$

Although it is possible to estimate the contributions of sunlit and shaded components variations with a sun-sensor geometry model for G (Colaizzi et al., 2010), the data requirements for its parameterization are not available using remote sensing. It has been argued that spatial variations at the landscape level are responsible for the no closure. Using Rn measurements, it has been shown that spatial variations with data of homogenous grassland fields are not significant (Twine et al., 2000), but with complex terrain these contributions (spatial heterogeneity and the use of Rn measurements at different heights) can explain a major part of the balance of energy closure (Stoy et al., 2013; Shao et al., 2014; Wohlfahrt and Tasser, 2015; Georg et al., 2016; Wohlfahrt et al., 2016).

Considering that albedo has major contributions to Rn, many authors are argued that with inclined surfaces it is necessary to correct Rn measurements (horizontally, nadir view) for the slope of the terrain (Leuwing et al., 2012; Wohlfahrt and Tasser, 2015). Rn nadir measurements in inclined surfaces are lesser than in horizontal ones (Fritschen and Quian, 1990; Nie et al., 1992) because of it is necessary to correct solar radiation for the slope of the surface (Fritschen and Quian, 1990; Nie et al., 1992; Leuning et al., 2012). These corrections show that the conventional Rn measurements in flat terrains are overestimated in complex topography or inclined surfaces. Despite the corrections for inclined surfaces, this approach is only a partial solution to the energy balance closure because it changes the geometry of the terrain and does not consider footprint areas adjustments for Rn.

Considering the arguments for the problem of footprint mismatch among components of energy and matter balance (equation 2), for any fixed time period, we can set c fixed in equation (18), so that the lack of closure is simply an issue (geometric version) of comparing measuring area between ellipses and circles. Since Rn always decreases value as the zenithal angle view increases, this situation ensures overestimating (Rn – G) in the energy balances.

5. Conclusions

The dependence of the components of net radiation — radiative temperature and albedo — on sun-sensor geometry is quantified by a simple modelling strategy involving the use of a single observation (additional to angular data) from remote sensors on board satellite platforms. The relationship between sun-sensor geometry and footprints of measurements made with the eddy covariance technique allows generalizing the sun-sensor geometry model to standardize energy balance footprints and account for the lack-of-closure issue.

The sun-sensor geometry model of Rn components presented shows good empirical adjustments with field measurements (albedo (%): $R^2 = 0.9971$, RMSE = 0.432; radiative temperature (°): $R^2 = 0.9967$, RMSE = 0.008). The one-parameter model can be parameterized using only one measurement and sun-sensor geometry data, letting to be used in an operational fashion.

After analyzing the implications of the developed model and measurements done on the field, along with footprint geometry, one conclusion associated with the energy balance closure problem is that it can be explained for the overestimations due to nadir view of Rn fluxes and the mismatch of its footprint with aerodynamic fluxes (latent water and sensible heat fluxes).

6. Data availability

All field data used to validate the sun-sensor geometry are available in http://pmcarbono.org/pmc/bases_datos/Base datos Footprint Albedo and Tr/

7. Acknowledgments

This research was conducted as part of the activities of the project Participatory multi-level EO-assisted tools for Irrigation water management and Agriculture Decision-Support (PLEIADES) with financial support from the European Commission.

8. References

Allen, R.G., M. Tasumi, and Trezza, R. (2007). Satellite-based energy balance for mapping evapotranspiration with internalized calibration (METRIC) – model. *Journal of irrigation and drainage engineering, 133 (4)*, 380-394. doi: 10.1061/(ASCE)0733-9437(2007)133:4(380)

Allen, R.G., Pereira, L.S., Raes, D., and M. Smith, M. (1998). Crop evapotranspiration: Guidelines for computing crop requirements. Irrigation and Drainage Paper No. 56. Rome, Italy: FAO. Available in http://www.fao.org/tempref/SD/Reserved/Agromet/PET/FAO_Irrigation_Drainage_Paper_56.pdf.

Anderson, M.C., Norman, J.M., Mecikalski, J.R., Otkin, J.P., and Kustas, W.P. (2007). A climatological study of evapotranspiration and moisture stress across the continental U. S. based on the thermal remote sensing: I Model formulation, Journal of Geophysical Research 112 doi:10.1029/2006JD007506

Anderson, M.C., Norman, J.M., Kustas, W.P., Houborg, R., Starks, P.J., and Agam, N. (2008). A thermal-based remote sensing technique for routine mapping of land-surface carbon, water and energy fluxes from field to regional scales. *Remote Sensing of Environment, 112(12), 4227–4241. https://doi.org/10.1016/j.rse.2008.07.009*

Aubinet, M., Grelle, A., Ibrom, A., Rannik, Ü., Moncrieff, J., Foken, T., et al. (1999). Estimates of the Annual Net Carbon and Water Exchange of Forests: The EUROFLUX Methodology. *Advances in Ecological Research*, 30(C), 113–175. https://doi.org/10.1016/S0065-2504(08)60018-5

Bala, G., Caldeira, K., Wickett, M., Phillips, T.J., Lobell, D.B., Delire, C., and Mirin, A. (2007). Combined climate and carbon-cycle effects of large-scale deforestation. *Proceedings of the National Academy of Sciences, 104 (16), 6550-6555. DOI: 10.1073/pnas.0608998104*

Baldocchi, D.D., Hicks, B.B., and Meyers, T.P. (1988). Measuring biosphere-atmosphere exchanges of biologically related gases with micrometeorological methods. *Ecology, 69*, 331-1340. doi:10.2307/1941631

Bastiaanssen, W. G. M., Menenti, M., Feddes, R. A., and Holtslag, A. A. M. (1998). A remote sensing surface energy balance algorithm for land (SEBAL): 1. Formulation. *Journal of Hydrology, 212–213(1–4), 198–212. https://doi.org/10.1016/S0022-1694(98)00253-4*

Bolaños-González, Martín A., Paz-Pellat, Fernando, Palacios-Vélez, Enrique, Mejía-Sáenz, Enrique, and Huete, Alfredo. (2007). Modelation of the sun-sensor geometry effects in the vegetation reflectance. Agrociencia, 41(5), 527-537. Available in http://www.scielo.org.mx/scielo.php?script=sci_arttext&pid=S1405-31952007000500527&lng=es&tlng=es

Bolaños González, Martín Alejandro, and Paz Pellat, Fernando. (2010). Modelación general de los efectos de la geometría de iluminación-visión en la reflectancia de pastizales. Revista mexicana de ciencias pecuarias, 1(4), 349-361. Available in http://www.scielo.org.mx/scielo.php?script=sci_arttext&pid=S2007-11242010000400004&lng=es&tlng=es

Brutsaerth, W. (1982). Evaporation into the Atmosphere: Theory, History and Applications. Reidel. Dordrecht: Reidel 299.

Cano González, A., F. Paz, M.I. Marín, E. López, J. Chávez, M. Bolaños y J.L. Oropeza. 2018. Factor de reflectancia bi-cónica en especies vegetales contrastantes: modelación de los ángulos cenitales. Terra Latinoamericana 36:105-119. https://doi.org/10.28940/terra.v36i2.226

Casiano, M., Paz, F., Zarco, A., Bolaños, M., and Palacios, E. (2012). Escalamiento espacial de medios heterogéneos espectrales usando invarianzas temporales. T*erra Latinoamericana,* 30(4), 315-326. Available in: https://www.redalyc.org/articulo.oa?id=57325814003

Chehbouni, A., Watts, C., Kerr, Y.H., Dedieu, G., Rodriguez, J.C., Santiago, F., Cayrol, P., Boulet, G., and Goodrich, D.C. (2000). Methods to aggregate turbulent fluxes over heterogenous surfaces: application to SALSA data set in Mexico. *Agricultural and Forest Meteorology, 105 (1-3)*, 133-144. https://doi.org/10.1016/S0168-1923(00)00185-4

Chehbouni, A., Nouvellou, Y., Lhomme, J.P., Watts, C., Boulet, G., Kerr, Y.H., et al. (2001). Estimation of surface sensible heat flux using dual angle observations of radiative surface temperature. *Agricultural and Forest Meteorology (2001) 108(1) 55-65.*DOI: 10.1016/S0168-1923(01)00221-0

Chen, B., Black, T.A., Coops, N.C., Hilker, T., Trofymow, J.A., and Morgenstern, K. (2009). Assessing tower flux footprint climatology and scaling between remotely sensed and eddy covariance measurements. *Boundary-Layer Meteorology, 130 (2)*, 137-167. https://doi.org/10.1007/s10546-008-9339-1

Chirouze, J., Boulet, G., Jarian, L., Fieuzal, R., Rodriguez, J.C., Exxahar, J., et al. (2014). Inter-comparison of four remote sensing based surface energy balance methods to retrieve surface evapotranspiration and water stress of irrigated fields in semi-arid climate. *Hydrology and Earth System Sciences, 18, 1165–1188.* https://doi.org/10.5194/hess-18-1165-2014, 2014

Colaizzi, P.D., S.A. O'Shaughnessy, P.H. Gowda, S.R. Evett, T.A. Howell, W.P. Kustas and M.C. Anderson. (2010). Radiometer footprint model to estimate sunlit and shaded components for row crops. Agronomy Journal 102:942-955. https://doi.org/10.2134/agronj2009.0393

Courault, D., Seguin, B., and Olioso, A. (2005). Review on estimation evapotranspiration from remote sensing data: From empirical to numerical modeling approaches. *Irrigation and Drainage System, 19 (3-4)*, 223-249. https://doi.org/10.1007/s10795-005-5186-0

Cuenca, J., and Sobrino, J.A. (2004). Experimental measurements for studying angular and spectral variation of thermal infrared emissivity. *Applied Optics, 43 (23)*, 4598-4602. https://doi.org/10.1364/AO.43.004598

Di Girolamo, L. (2003). Generalizing the definition of the bi-directional reflectance function. Remote Sensing of Environment 88:479-482. https://doi.org/10.1016/j.rse.2003.07.004

Du, Y., B. Cao, H. Li, Z. Bian, B. Qin, Q. Xiao, q. Liu, Y. Zeng and Z. Su. (2020). Modeling directional brightness temperatura (DBT) over crop

canopy with effects of intra-row heterogeneity. Remote Sensing. 12, 2667, DOI:10.3390/2667Rs1217

Foken, T. (2008). The energy balance closure problem: an overview. Ecological Applications 18::1351-1367. https://doi.org/10.1890/06-0922.1

Fritschen, L. and P. Quian. (1990). Net radiation, sensible and latent heat flux densities on slopes computed by the energy balance method. Boundary Layer Meteorology 53:163-171. https://doi.org/10.1007/BF00122468

Garatuza-Payan J., Pinker, R., Shuttleworth, W.J., and Watts, C.J. (2001). Solar radiation and evapotranspiration in northern Mexico estimated from remotely sensed measurements of cloudiness. *Hydrological Sciences Journal, 46 (3), 465-478. DOI: 10.1080/02626660109492839*

Garatuza-Payan J., Shuttleworth, W.J., Encinas, D., McNeil, D., Stewart, J.B., de Bruin, H., and Watts, C. (1998). Measurement and modelling evaporation for irrigated crops in north-west Mexico. *Hydrological Processes, 12*, 1397-1418. doi:10.1002/(SICI)1099-1085(199807)12:9<1397::AID-HYP644>3.0.CO;2-E

Gowda, P.H., Chavex, J.L., Colaizzi, P.D., Evett, S.R., Howell, T.A., and Tolk, J.A. (2008). ET mapping for agricultural water management: present status and challenges. *Irrigation Science, 26*, 223-237. https://doi.org/10.1007/s00271-007-0088-6

Idso, S.B., J.K. Aase and R.D. Jackson. (1975). Net radiation – soil heat flux relations as influenced by soil water content variations. Boundary – Layer Meteorology 9:113-122. https://doi.org/10.1007/BF00232257

Jiang, L., H. Yang, X. Li and X. Ding. (2001). Modeling effective directional emissivity of row crops. IEEE Xplore. Conference: Geoscience and Remote Sensing Symposium, 2001. IGARSS '01. IEEE 2001 International. Volume: 4 DOI:10.1109/IGARSS.2001.977135

Jupp, D.L.B. (1998). Directional radiance and emissivity measurement model for remote sensing of the surface energy balance. *Environmental Modelling and Software,* 13(3–4), 341–351. https://doi.org/10.1016/S1364-8152(98)00039-5

Kalma, J.D., McVicar, T.R., and Cabe, M.F. (2008). Estimating land surface evaporation: a review of methods using remotely sensed surface temperature data. *Surveys in Geophysics, 29 (4-5)*, 421-429. https://doi.org/10.1007/s10712-008-9037-z

Kimes, D.S. (1980). Effect of vegetation canopy structure on remotely sensed canopy temperatures. *Remote Sensing of Environment,* 10(3), 165–174. https://doi.org/10.1016/0034-4257(80)90020-6

Lecrlerc, M.Y., and Thurtell, G.W. (1990). Footprint prediction of scalar fluxes using a Markovian analysis. *Boundary-Layer Meteorology, 52*, 247-258. Available in https://www.aminer.cn/pub/53e999e7b7602d970222d7e7/footprint-prediction-of-scalar-fluxes-using-a-markovian-analysis.

Leuning, R., E. van Gorsel, W.J. Massman and P.R. Isacc. (2012). Reflections on the Surface energy imbalance problem. Agricultural and Forest Meteorology 156:65-74. https://doi.org/10.1016/j.agrformet.2011.12.002

Liang, S. (2000). Narrowband to broadband conversions of land surface albedo: I Algorithms. *Remote Sensing of Environment, 76(2), 213–238. https://doi.org/10.1016/S0034-4257(00)00205-4*

Liang, S., Shuey, C.J., Russ, A.L., Fang, H., Chen, M., Walthall, C.L., Daughtry, et al. (2002). Narrowband to broadband conversions of land surface albedo: II Validation. *Remote Sensing of Environment, 84(1), 25–41. https://doi.org/10.1016/S0034-4257(02)00068-8*

Marcolla, B. and A. Cescatti. (2018). Geometry of the hemispherical radiometric footprint over plant canopies. Theor. Appl. Climatol. 134:981-990. https://doi.org/10.1007/s00704-017-2326-z

Mathias, A.D., Yates, S.R., Zhang, R., and Warrick, A.W. (1987). Radiant temperatures of sparse plant canopies and soil using IR thermometry. *IEEE transactions on geoscience and remote sensing, 25 (4)*, 516-520. DOI: 10.1109/TGRS.1987.289723

Mauder, M., T. Foken and J. Cuxart. (2020). Surface-energy-balance closure over land: a review. Boundary-Layer Meteorology 177:395-426. https://doi.org/10.1007/s10546-020-00529-6

Medrano-Ruedaflores, E.R., F. Paz-Pellat, J.L. Oropeza-Mota, J.R. Valdez-Lazalde y M. Bolaños-González. 2013. Evaluación de un modelo de la BRDF a partir de simulaciones con modelos semi-empíricos lineales (SEL). Terra Latinoamericana 31:181-192. Available in: http://www.scielo.org.mx/scielo.php?script=sci_abstract&pid=S0187-57792013000400181&lng=es&nrm=iso

Monteith, J.l., and Unsworth, M.H. (1990). *Principles of Environmental Physics*. London: Eduard Arnold

Nemani, R., Keeling, C., Hashimoto, H., Jolly, W., Piper, S., Tucker, C., Myneni, R., & Running, S. (2003). Climate-driven increases in global terrestrial net primary production from 1982 to 1999. *Science, 300 (5625)*, 1560-1563. DOI: 10.1126/science.1082750

Nie, d., T. Demetriades-Shah and E.T. Kanemasu. (1992). Surface energy fluxes on four slope sites during FIFE 1988. Journal of Geophysical Research 97:18641-18649

Pascual, F., Paz, F., and Bolaños, M. (2012). Estimación de biomasa aérea en cultivos con sensores remotos. *Terra Latinoamericana,* 30(1), 17-28. Available in http://www.scielo.org.mx/scielo.php?script=sci_arttext&pid=S0187-57792012000100017&lng=es&tlng=es

Paz, F. (2018). Estimación de la cobertura aérea de la vegetación herbácea usando sensores remotos. Terra Latinoamericana 36:239-259.

https://doi.org/10.28940/terra.v36i3.399

Paz, F., A. Cano, M. Bolaños, J. Chávez, M.I. Marín y E. Romero. 2018. Factor de reflectancia bi-cónica en especies vegetales contrastantes: modelación global. Terra Latinoamericana 36:61-73. https://doi.org/10.28940/terra.v36i1.222

Paz, F. and M.I .Marín. (2019). Desarrollo de un modelo genérico de footprint para sensores estáticos del sistema suelo-vegetación. Terra Latinoamericana 37:27-34. https://doi.org/10.28940/tl.v37i1.414

Paz, F. y E. Medrano. 2015. Patrones espectrales multi-angulares de clases globales de coberturas del suelo usando el sensor remoto POLDER-1. Terra Latinoamericana 33:129-137. Available in: http://www.scielo.org.mx/scielo.php?script=sci_arttext&pid=S0187-57792015000200129

Paz, F. y E. Medrano. 2016. Discriminación de coberturas del suelo usando datos espectrales multi-angulares del sensor POLDER-1: alcances y limitaciones. Terra Latinoamericana 34:187-200. Available in: http://www.scielo.org.mx/scielo.php?script=sci_arttext&pid=S0187-57792016000200187

Priestley, C.H.B., and Taylor, R.J. (1972). On the assessment of surface heat flux and evaporation using large scale parameters. *Monthly Weather Review, 100 (2)*, 81-92. DOI:10.1175/1520-0493(1972)100<0081:OTAOSH>2.3.CO;2

Ranson, K.J., Irons, J.R., and Daughtry, C.S.T. (1991). Surface albedo from bidirectional reflectance. *Remote Sensing of Environment,* 35(2–3), 201–211. https://doi.org/10.1016/0034-4257(91)90012-U

Reyes, M., Paz, F., Casiano, M., Pascual, F., Marín, M.I., and Rubiños, E. (2011). Characterization of stress effect using spectral vegetation indexes for the estimate of variables related to aerial biomass. *Agrociencia,* 45(2), 221-233. Available in http://www.scielo.org.mx/scielo.php?script=sci_arttext&pid=S1405-31952011000200007&lng=es&tlng=es

Roerink, G.J., Su, B., and Menenti, M. (2000). S-SEBI a simple remote sensing algorithm to estimate the surface energy balance. *Physics and Chemistry of the Earth, Part B: Hydrology, Oceans and Atmosphere,* 25(2), 147–157. https://doi.org/10.1016/S1464-1909(99)00128-8

Salisbury, J.W., and d'Aria, D.M. (1992). Emissivity of terrestrial materials in the 8-14 m atmospheric window. *Remote Sensing of Environment,* 42 (2), 83-106. https://doi.org/10.1016/0034-4257(92)90092-X

Santanello, J.A. and M.A. Friedl. (2003). Diurnal covariation in soil heat flux and net radiation. Journal of Applied Meteorology 42:851-862. https://doi.org/10.1175/1520-0450(2003)042%3C0851:DCISHF%3E2.0.CO;2

Schmid, H.P. (1997). Experimental design for flux measurements: matching scales of observations and fluxes. Agricultural and Forest Meteorology 87:179-200.

Schmid, H.P. (2002). Footprint modeling for vegetation atmosphere exchange studies: a review and perspective. *Agricultural and Forest Meteorology,* 113(1–4), 159–183. https://doi.org/10.1016/S0168-1923(02)00107-7

Shao, C., L. Li and J. Chen. (2014). Spatial variation of net radiation and its contribution to energy balance closures in grassland ecosystems. Ecological Processes 3:7. https://doi.org/10.1186/2192-1709-3-7

Smith, J.A., and Ballard, J.R. (2001). Thermal infrared hot spot and dependence on canopy geometry. *Optical Engineering* 40(8), 1435-1437. https://doi.org/10.1117/1.1387990

Snyder, W.C. (1998). Reciprocity of the bidirectional reflectance distribution function (BRDF) in measurements and models of structured surfaces. IEEE Transactions on Geosciences and Remote Sensing 36:685-693. doi: 10.1109/36.662750

Snyder, W.C., and Wan, Z. (1998). BRDF models to predict spectral reflectance and emissivity in the thermal infrared. *IEEE Transactions on Geoscience and Remote Sensing*, vol. 36 (1), 214-225. https://doi.org/10.1109/36.655331

Sobrino, J.A., Jimenez, J.C., and Verhoef, W. (2005). Canopy directional emissivity: comparison between models. *Remote Sensing of Environment, 99(3), 304–314. https://doi.org/10.1016/j.rse.2005.09.005*

Stoy, P.C., M. Mauder, T. Foken, B. Marcolla, E. Boegh, A. Ibrom, et al. (2013). A data-drien análisis of energy balance closure across FLUXNET research sites: the role of landscape scale heterogeneity. Agricultural and Forest Meteorology Volume 171/172 DOI:101016/j.agrformet.2012.11.004

Su, Z. (2002). The surface energy balance system (SEBS) for turbulent heat fluxes. Hydrology and Earth System Sciences Discussions 6(1), 85-100. https://doi.org/10.5194/hess-6-85-2002

Twine, T.E., W.P. Kustas, J.M. Norman, D.R. Cook, P.R. Houser, T.P. Meyers, et al. (2000). Correcting Eddy-covariance flux underestimates over grassland. Agricultural and Forest Meteorology 103:279-300. https://doi.org/10.1016/S0168-1923(00)00123-4

Verma, S.B. (1990). Micrometeorological methods for measuring surface fluxes of mass and energy. *Remote Sensing Reviews,* 5 (1), 99-115, DOI: 10.1080/02757259009532124

Vesala, T., N. Kljun, Ü. Rannik, J. Rinne, A. Sogachev, T. Markkanen, et al. (2008). Flux and concentration footprint modelling: state of the art. Environmental Pollution 152:653-666. https://doi.org/10.1016/j.envpol.2007.06.070

Wanner W., Li, X., and Strahler, A.H. (1995). On the derivation of kernels for kernel-driven models of bidirectional reflectance. *Journal of Geophysics Research, 100(D10), 21077– 21089, doi:10.1029/95JD02371*

Wilson, K., Goldstein, A., Falge, E., Aubinet, M., Baldocchi, D., Berbigier, P., et al. (2002). Energy balance closure at FLUXNET sites. *Agricultural and Forest Meteorology,* 113(1–4), 223–243. https://doi.org/10.1016/S0168-1923(02)00109-0

Wohlfahrt, G. and E. Tasser. (2015). A mobile system for quantifying the spatial variability of the Surface energy balance: design and application. Int. J. Biometeorol. 59:617-627. https://doi.org/10.1007/s00484-014-0875-8

Wohlfahrt, G., A. Hammerle, G. Niedrist, K. Scholtz, E. Tomelleri and P. Zhao. (2016). On the energy balance closure and net radiation in complex terrain. Agricultural and Forest Meteorology 226-227:37-49. https://doi.org/10.1016/j.agrformet.2016.05.012

Zeng, Z., L. Peng, and S. Piao. (2018). Response of terrestrial evapotranspiration to Earth's greening. Current Opinion in Environmental Sustainability. Elsevier B.V. https://doi.org/10.1016/j.cosust.2018.03.001

Zhao, F., X. Gu, W. Verhoef, Q. Wang, T. Yu, Q. Liu, H. Huang, W. Qin, L. Chen and H. Zhao. (2010). A spectral directional reflectance model f row crops. Remote Sensing of Environment 114:265-285. https://doi.org/10.1016/j.rse.2009.09.018